Dielectric and pyroelectric properties of barium strontium titanate films on orthorhombic substrates with (110)//(100) epitaxy

G. Akcay, I. B. Misirlioglu,[a] and S. P. Alpay[b]
Department of Materials Science and Engineering and Institute of Materials Science, University of Connecticut, Storrs, Connecticut 06269

(Received 23 January 2007; accepted 9 March 2007; published online 24 May 2007)

The role of anisotropic misfit strains on the spontaneous polarization, dielectric properties, and pyroelectric response of (110) oriented $Ba_{0.6}Sr_{0.4}TiO_3$ (BST 60/40) thin films on (100) orthorhombic substrates is analyzed theoretically. The anisotropic in-plane strain state and the rotation of the elastic and the electrostrictive constants of the BST 60/40 films result in strongly directional and unique properties, different from BST 60/40 films on cubic substrates with $(100)_{BST}//(100)_{substrate}$ epitaxy. The thermodynamic formalism also incorporates the thickness dependence of the internal stress state due to the anisotropic relaxation of epitaxial stresses through the formation of misfit dislocations along the two in-plane directions. In particular, the model is applied to (110) BST 60/40 ferroelectric films on (100) $NdGaO_3$ orthorhombic substrates. A more generalized analysis treating the in-plane misfit strains as parameters shows that ferroelectric phases that cannot be observed in single-crystal perovskite ferroelectrics can be stabilized due to the reduction in the symmetry induced by the anisotropic strain state. © *2007 American Institute of Physics*. [DOI: 10.1063/1.2729474]

I. INTRODUCTION

Thin films of barium strontium titanate ($Ba_xSr_{1-x}TiO_3$, BST) are of great technological interest due to their desirable ferroelectric and dielectric properties. Their high dielectric response offers the potential of replacing the current silicon oxide and nitride dielectrics in the next generation dynamic random access memories (DRAM) which require higher integration densities. The dielectric constant of these materials is strongly dependent on the applied electric field. This is an attractive property for frequency-agile microwave electronic components, including phase shifters, varactors, tunable filters, and antennas. Furthermore, BST compounds have high pyroelectric coefficients and thus can be used in infrared (IR) detection, most particularly, as the active sensing elements of focal plane arrays in thermal imaging systems. The reason for high dielectric and pyroelectric properties BST compositions with $0.3 \leq x \leq 0.5$ is that the addition of Sr to $BaTiO_3$ as to substitute for Ba^{+2} in the prototypical perovskite unit cell results in a decrease in the ferroelectric-paraelectric phase transformation temperature (T_C) down to temperatures close to room temperature (RT, 25 °C). For example, for $Ba_{0.6}Sr_{0.4}TiO_3$ (BST 60/40), the bulk T_C is just below RT (5 °C). Thus, compositions in the $Ba_{0.7}Sr_{0.3}TiO_3$ (BST 70/30) to $Ba_{0.5}Sr_{0.5}TiO_3$ (BST 50/50) range have attracted significant interest as material systems of choice for such applications.

Much of the work concerning the high dielectric tunability and pyroelectric applications of BST films form consists of growing these on substrates with cubic (or pseudo-cubic) lattices such as Si, MgO, $SrTiO_3$, and $LaAlO_3$.[1–11] Theoretical models have been devised to understand the relation between the internal stresses (or strains) and the electrical and electromechanical properties of BST films.[12–14]

Cubic substrates generate internal stresses with equal orthogonal components along the in-plane directions and result in identical polarization components along the principal directions in a plane parallel to the film-substrate interface. Recently, in a series of experimental studies Simon *et al.*[15–17] showed that BST 60/40 grown on orthorhombic $NdGaO_3$ (NGO) substrates have strong directional electrical properties and these properties can be manipulated by varying the film thickness. Experimental findings indicate that BST 60/40 films on NGO substrates favor $(110)_{BST}//(100)_{NGO}$ epitaxy to minimize in-plane misfit.[16] Structurally, the strain relaxation of the BST 60/40 films grown on NGO substrates via the formation of misfit dislocations was also investigated. Two different critical thicknesses for misfit dislocation formation were reported in the film along principal in-plane directions.[16] The dielectric permittivity and tunability of these films as a function of film thickness and applied electrical fields were measured.[15,17] The relative small-signal dielectric constant of BST 60/40 films along $[1\bar{1}0]_{BST}$ was found to be varying from 125 at 150 nm film thickness to 370 at 1200 nm film thickness, with a maximum of 500 at 600 nm. 75 nm thick films displayed a markedly different behavior than films thicker than 150 nm. A maximum dielectric response of 270 was observed along $[\bar{1}11]:[1\bar{1}1]_{BST}$ while the minimum occurred along $[1\bar{1}0]_{BST}$. The dielectric tunability of BST 60/40 films on NGO at 5 kV/mm displayed a maximum at different film thicknesses in different directions. 600 nm thick films wherein strains along $[1\bar{1}0]_{BST}$ and $[001]_{BST}$ are mostly relieved, tunability was found to be at its maximum, 54% at 5 kV/mm.

[a]Current address: Max Planck Institute for Microstructure Physics, Weinberg, 06120, Halle-Saale, Germany.
[b]Author to whom correspondence should be addressed; electronic mail: p.alpay@ims.uconn.edu

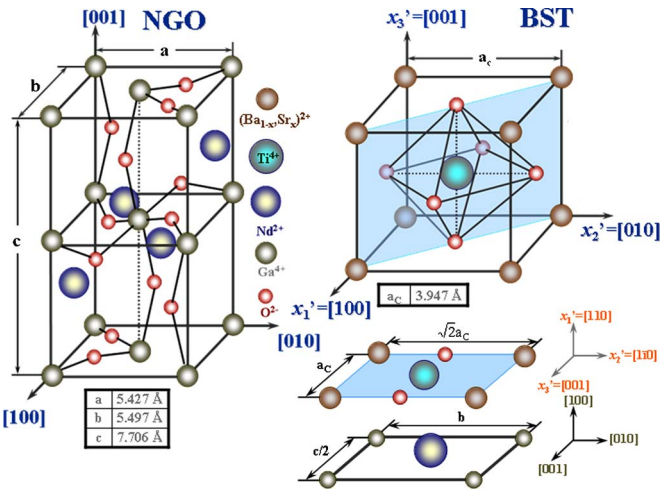

FIG. 1. (Color online) Microstructures of the ferroelectric thin film, BST 60/40 and anisotropic substrate, NGO. Epitaxy of BST 60/40 growth on NGO is also shown: $(110)_{BST}//(100)_{NGO}$ (Refs. 15–17).

Theoretically, the role of anisotropic in-plane misfit strains on the phase transformation characteristics and the dielectric response of (100) $PbTiO_3$ and (100) $Pb_{0.35}Sr_{0.65}TiO_3$ on (100) orthorhombic substrates has been addressed.[18] The analysis shows that the in-plane strain anisotropy may lead to the formation of phases that do not form in films on cubic substrates. While this epitaxial relation holds $Pb_{0.35}Sr_{0.65}TiO_3$ on NGO,[19] such a formalism has to be modified to be employed for BST on NGO substrates since the preferred epitaxy by which BST grows on NGO is given by $(110)_{BST}//(100)_{NGO}$. This epitaxial relation creates a different reduction in the point group symmetry compared to $(100)_{BST}//(100)_{NGO}$. Recently, we developed a preliminary thermodynamic model based on the Landau-Devonshire (LD) theory of phase transformations to understand the dielectric tunability of BST 60/40 ferroelectric thin films on orthorhombic NGO substrates with $(110)_{BST}//(100)_{NGO}$ epitaxy.[20] This analysis takes into account the thickness dependence of the anisotropic in-plane strains as well as the thermal strains that develop during subsequent cooling to room temperature. It was shown that this model can be further improved using two similar theoretical formalisms.[21,22] In this report, we build upon these findings and provide a comprehensive analysis of the dielectric and pyroelectric properties of BST 60/40 film on NGO substrates as a function of the film thickness. These results are then generalized for (110) BST on any (100) orthorhombic substrate by evaluating the components of the polarization vector of BST as a function of the anisotropic misfit. This approach shows that ferroelectric phases with monoclinic and triclinic symmetry can be stabilized in this system due to the reduction in the symmetry induced by the anisotropic strain state.

II. THEORY

Consider a (110) oriented BST 60/40 film on a thick (100) oriented NGO substrate (Fig. 1). The in-plane misfit strains in the epitaxial coordinate system (x_1, x_2, x_3) along $[001]_{BST}$ and $[1\bar{1}0]_{BST}$ are defined as

$$u_{11} = \frac{a_{[001]_{NGO}} - d_{[001]_{BST}}}{a_{[001]_{NGO}}} \tag{1}$$

and

$$u_{22} = \frac{a_{[010]_{NGO}} - d_{[1\bar{1}0]_{BST}}}{a_{[010]_{NGO}}}, \tag{2}$$

respectively, where $a_{[001]_{NGO}}$ and $a_{[010]_{NGO}}$ are the lattice parameters of the NGO substrate in the given directions, and $d_{[001]_{BST}}$ and $d_{[1\bar{1}0]_{BST}}$ are the lattice parameters along [001] and $[1\bar{1}0]$ of unconstrained (bulk) BST 60/40 in the paraelectric state at room temperature (RT).

The lattice parameters of BST 60/40 are 0.3965 and 0.5607 nm along the directions of $[001]_{BST}$ and $[1\bar{1}0]_{BST}$ giving rise to misfit strains, $u_{11}=-2.79\%$ and $u_{22}=-1.93\%$, respectively, at RT for pseudomorphic films.[16] The corresponding lattice constants of NGO at RT are 0.3858 and 0.5501 nm along $[001]_{NGO}$ and $[010]_{NGO}$, respectively[16] (see Fig. 1). In order to incorporate dislocation relaxation at the deposition temperature $T_G=600\ ^\circ C$ with increasing film thickness, we use critical thickness for misfit dislocation formation data from Simon *et al.*[15,16] The critical thicknesses $h_{[001]_{BST}}$ and $h_{[1\bar{1}0]_{BST}}$ are 5 and 7 nm, respectively, which were determined using the Matthews-Blakeslee criteria.[23] Thus, the effective misfit strain as a function of misfit dislocation density along $[001]_{BST}$ and $[1\bar{1}0]_{BST}$ can be calculated through the effective NGO lattice parameter at RT as[24,25]

$$\bar{u}_{11}(\mathrm{RT}) = \frac{\bar{a}_{[001]_{NGO}}(\mathrm{RT}) - d_{[001]_{BST}}(\mathrm{RT})}{\bar{a}_{[001]_{NGO}}(\mathrm{RT})}, \tag{3a}$$

$$\bar{u}_{22}(\mathrm{RT}) = \frac{\bar{a}_{[010]_{NGO}}(\mathrm{RT}) - d_{[1\bar{1}0]_{BST}}(\mathrm{RT})}{\bar{a}_{[010]_{NGO}}(\mathrm{RT})}, \tag{3b}$$

respectively, where $\bar{a}_{[001]_{NGO}}$ and $\bar{a}_{[010]_{NGO}}$ are the effective lattice parameters of NGO along the corresponding directions at RT, which can be defined as

$$\bar{a}_{[001]_{NGO}}(\mathrm{RT}) = \frac{a_{[001]_{NGO}}(\mathrm{RT})}{\rho_{[001]_{BST}}(T_G)\cdot a_{[001]_{NGO}}(\mathrm{RT}) + 1}, \tag{4a}$$

$$\bar{a}_{[010]_{NGO}}(\mathrm{RT}) = \frac{a_{[010]_{NGO}}(\mathrm{RT})}{\rho_{[1\bar{1}0]_{BST}}(T_G)\cdot a_{[010]_{NGO}}(\mathrm{RT}) + 1}. \tag{4b}$$

Here, $\rho_{[001]_{BST}}$ and $\rho_{[1\bar{1}0]_{BST}}$ are the dislocation densities of BST 60/40 in the given directions

$$\rho_{[001]_{BST}}(T_G) = \frac{u_{11}(T_G)}{a_{[001]_{NGO}}(T_G)}\left(1 - \frac{h_{[001]_{BST}}}{h}\right), \tag{5a}$$

$$\rho_{[1\bar{1}0]_{BST}}(T_G) = \frac{u_{22}(T_G)}{a_{[010_{NGO}]}(T_G)}\left(1 - \frac{h_{[1\bar{1}0]_{BST}}}{h}\right), \tag{5b}$$

where h is the thickness of the BST 60/40 film. The values of lattice parameters of NGO at T_G along the given directions can be calculated using the thermal expansion coefficients (TECs) of the film and the substrate along the corresponding

directions. TECs of NGO are $5.6\times10^{-6}\,\mathrm{K}^{-1}$ and $11.6\times10^{-6}\,\mathrm{K}^{-1}$ along $[010]_{\mathrm{NGO}}$ and $[001]_{\mathrm{NGO}}$, respectively, and the TEC of BST 60/40 is $10.5\times10^{-6}\,\mathrm{K}^{-1}$ along $\langle100\rangle$.[16]

Having found the misfit strains in the epitaxial coordinate system (x_1, x_2, x_3), we can evaluate the corresponding elastic strain, $\bar{u}_{33}$ along $[110]_{\mathrm{BST}}$ (x_3) by using the condition of

$$\sigma_{33} = c_{31}u_{11}^T + c_{32}u_{22}^T + c_{33}u_{33}^T = 0. \tag{6}$$

Here c_{ijkl} (c_{ij} in Voigt notation) is the elastic stiffness tensor in the epitaxial coordinate system (x_1, x_2, x_3) and can be determined in terms of the pseudocubic BST 60/40 elastic stiffness tensor (C_{mnop}) by using a tensor transformation

$$c_{ijkl} = a_{im}^{-1}a_{jn}^{-1}a_{ko}^{-1}a_{lp}^{-1}C_{mnop}, \tag{7}$$

where a_{im}^{-1}, a_{jn}^{-1}, a_{ko}^{-1}, and a_{lp}^{-1} are the terms of the inverse of the rotation matrix defined as

$$a = \begin{bmatrix} 0 & \sqrt{2}/2 & \sqrt{2}/2 \\ 0 & -\sqrt{2}/2 & \sqrt{2}/2 \\ 1 & 0 & 0 \end{bmatrix} x_i' \Rightarrow x_i. \tag{8}$$

This rotational operation transforms tensor quantities from and to the epitaxial and pseudo-cubic coordinate systems of BST 60/40. In Eq. (6), the total strain u_{11}^T in the epitaxial coordinate system (x_1, x_2, x_3) of the film is the sum of the polarization-free effective misfit, $\bar{u}_{ij}$, and self-strains, u_{ij}^0 expressed as

$$u_{ij}^T = \bar{u}_{ij} + u_{ij}^0, \tag{9}$$

where $i,j=1, 2, 3$. The self-strain of the ferroelectric phase transformation can be determined as a function of the electrostrictive coefficients q_{ijkl} and polarization P_i of BST 60/40 in epitaxial coordinates

$$u_{ij}^0 = P_i \cdot q_{ijkl} \cdot P_l, \tag{10}$$

where q_{ijkl} can be assessed in terms of well-known pseudocubic BST 60/40 electrostrictive tensor (Q_{mnop}) via

$$q_{ijkl} = a_{im}^{-1}a_{jn}^{-1}a_{ko}^{-1}a_{lp}^{-1}Q_{mnop}. \tag{11}$$

Using Eqs. (6)–(11), the corresponding elastic strain $\bar{u}_{33}$ along $[110]_{\mathrm{BST}}$ (x_3) can be evaluated as a function of polarization in the epitaxial coordinates (P_i)

$$\bar{u}_{33} = f(P_i), \tag{12}$$

and with the help of another tensor transformation, it can be expressed in terms of polarization defined in the pseudocubic coordinates such that

$$P_i = a_{ij}^{-1}P_j' \Rightarrow \bar{u}_{33} = f(P_i'). \tag{13}$$

This results in a misfit strain tensor given by

$$\bar{u} = \begin{bmatrix} \bar{u}_{11} & 0 & 0 \\ 0 & \bar{u}_{22} & 0 \\ 0 & 0 & \bar{u}_{33} \end{bmatrix}, \tag{14}$$

in the epitaxial coordinate system.

Now that the effective misfit strains $\bar{u}_{11}$ and $\bar{u}_{22}$ along x_1 and x_2, respectively, and the corresponding elastic strain, $\bar{u}_{33}$ along x_3 in the epitaxial coordinate system are determined, we utilize the rotational operator [Eq. (8)] to transform the effective misfit data of the epitaxial coordinate system (x_1, x_2, x_3) into that of the pseudocubic coordinate system (x_1', x_2', x_3') via

$$\bar{u}_{ij}' = a_{im}a_{jn}\bar{u}_{mn}. \tag{15}$$

Thus, the pseudocubic effective misfit strain matrix can be written in terms of epitaxial values, such that

$$\bar{u}' = \begin{bmatrix} \bar{u}_{11}' & \bar{u}_{12}' & 0 \\ \bar{u}_{21}' & \bar{u}_{22}' & 0 \\ 0 & 0 & \bar{u}_{33}' \end{bmatrix} = \begin{bmatrix} \frac{\bar{u}_{22}}{2} + \frac{\bar{u}_{33}}{2} & -\frac{\bar{u}_{22}}{2} + \frac{\bar{u}_{33}}{2} & 0 \\ -\frac{\bar{u}_{22}}{2} + \frac{\bar{u}_{33}}{2} & \frac{\bar{u}_{22}}{2} + \frac{\bar{u}_{33}}{2} & 0 \\ 0 & 0 & \bar{u}_{11} \end{bmatrix}. \tag{16}$$

Once the strain state is established, a thermodynamic analysis based on the LD theory of phase transformations can be carried out. The total free energy density of the film in the pseudocubic coordinates follows from:

$$G_\Sigma = G_0 + G_L + G_{EL} + G_{ES}, \tag{17}$$

where G_0 is the energy of the paraelectric state. In Eq. (17), G_L, G_{EL}, and G_{ES} define the energy in the ferroelectric state, the elastic energy of the internal stresses, and the electrostatic energy due to an applied electric field E_i', respectively, such that

$$G_L = \alpha_i P_i'^2 + \alpha_{ij}P_i'^2P_j'^2 + \alpha_{ijk}P_i'^2P_j'^2P_k'^2, \tag{18}$$

$$G_{EL} = \tfrac{1}{2}u_{ij}'^T \cdot C_{ijkl} \cdot u_{kl}'^T, \tag{19}$$

$$G_{ES} = -E_i' \cdot P_i', \tag{20}$$

where α_i, α_{ij}, and α_{ijk} are the dielectric stiffness coefficients, P_i' is the polarization vector, and C_{ijkl} are the elastic coefficients at constant polarization of stress-free and unclamped pseudocubic BST. All of these terms are defined in the pseudocubic coordinate system (x_1', x_2', x_3'). After some rearrangement, we obtain

$$\begin{aligned} G_\Sigma = {} & \bar{\alpha}_1(P_1'^2 + P_2'^2) + \bar{\alpha}_3P_3'^2 + \bar{\alpha}_{11}(P_1'^4 + P_2'^4) + \bar{\alpha}_{33}P_3'^4 \\ & + \bar{\alpha}_{12}P_1'^2P_2'^2 + \bar{\alpha}_{13}(P_1'^2P_3'^2 + P_2'^2P_3'^2)\beta_1(P_2'P_1'^3 \\ & + P_1'P_2'^3) + \beta_2P_2'P_2' + \beta_3P_3'^2P_2'P_1' + \bar{G}_{EL} - E_3P_3' \\ & - E_2P_2' - E_1'P_1', \end{aligned} \tag{21}$$

with $\bar{\alpha}_i$ and $\bar{\alpha}_{ij}$ being renormalized dielectric stiffness coefficients which are modified by C_{ijkl}, $\bar{u}_{11}$ and $\bar{u}_{22}$ [substituting the misfit values after tensor transformation, see Eqs. (15) and (16)] to reflect the presence of internal strain and its coupling to the polarization via electrostriction as well as the clamping effect of the substrate. Here, β_i are the coefficients of the free energy terms which appear due to the resultant shear strains in the pseudo-cubic coordinate system (x_1', x_2', x_3'). The coefficients of Eq. (21) are given by

$$\bar{\alpha}_1 = \alpha_1 - \eta\{[C_{11}^2 + C_{11}(C_{12}+2C_{44}) - 2C_{12}^2]Q_{12}\bar{u}_{11} + 2C_{12}C_{44}(Q_{12}+Q_{11})\bar{u}_{11} + 2C_{44}[C_{11}(Q_{11}+Q_{12}) + C_{12}(3Q_{12}+Q_{11})]\bar{u}_{22}\}, \quad (22a)$$

$$\bar{\alpha}_3 = \alpha_1 - \eta\{[C_{11}^2 + C_{11}(C_{12}+2C_{44}) - 2C_{12}^2]Q_{11}\bar{u}_{11} + 4C_{12}C_{44}Q_{12}\bar{u}_{11} + 4C_{44}[C_{12}(Q_{11}+Q_{12}) + C_{12}Q_{12}]\bar{u}_{22}\}, \quad (22b)$$

$$\bar{\alpha}_{11} = \alpha_{11} + \tfrac{1}{2}\eta\{[C_{11}^2 + C_{44}(5C_{12}+3C_{11}) + C_{11}C_{12} - 2C_{12}^2]Q_{12}^2 + 2(3C_{12}+C_{11})C_{44}Q_{11}Q_{12} + C_{44}(C_{11}+C_{12})Q_{11}^2\}, \quad (22c)$$

$$\bar{\alpha}_{33} = \alpha_{11} + \tfrac{1}{2}\eta\{[C_{11}^2 + C_{11}(2C_{44}+C_{12}) - 2C_{12}^2]Q_{11}^2 + 8C_{12}C_{44}Q_{11}Q_{12} + 4C_{44}(C_{11}+C_{12})Q_{12}^2\}, \quad (22d)$$

$$\bar{\alpha}_{12} = \alpha_{12} - \eta\{(C_{11}+C_{12})C_{44}Q_{11}^2 + 2C_{44}(C_{11}+3C_{12})Q_{11}Q_{12} + [C_{11}^2 - 2C_{12}^2 + C_{44}(3C_{11}+5C_{12}) + C_{11}C_{12}]Q_{12}^2 + 8C_{44}Q_{44}^2(C_{12}+C_{11})\}, \quad (22e)$$

$$\bar{\alpha}_{13} = \alpha_{12} - \eta\{2C_{12}C_{44}Q_{11}^2 + [C_{11}^2 + 4C_{44}(C_{11}+C_{12}) + C_{11}C_{12} - 2C_{12}^2]Q_{11}Q_{12} + 2C_{44}(C_{11}+3C_{12})Q_{12}^2\}, \quad (22f)$$

$$\beta_1 = -4\eta Q_{44}C_{44}[(C_{11}+3C_{12})Q_{12} + (C_{11}+C_{12})Q_{11}], \quad (22g)$$

$$\beta_2 = 8\eta Q_{44}C_{44}[C_{12}\bar{u}_{11} + (C_{11}+C_{12})\bar{u}_{22}], \quad (22h)$$

$$\beta_3 = -8\eta Q_{44}C_{44}[(C_{11}+C_{12})Q_{12} + C_{12}Q_{11}]. \quad (22i)$$

In the above relations, $\alpha_1 = (T - T_C)/2\varepsilon_0 C$, T_C and C are the Curie-Weiss temperature and constant of stress-free and unclamped ferroelectric, and ε_0 is the permittivity of free space. The coefficient η in Eqs. (22a)–(22i) is given by $\eta = 1/(C_{11}+C_{12}+2C_{44})$. $\bar{G}_{EL}$ in Eq. (20) is the polarization-free elastic energy of the BST in the paraelectric state

$$\bar{G}_{EL} = \tfrac{1}{2}\eta\{C_{44}[2C_{11}\bar{u}_{11}^2 + 8C_{12}\bar{u}_{11}\bar{u}_{22} + 4(C_{11}+C_{12})\bar{u}_{22}^2] + (C_{11}^2 + C_{11}C_{12} - 2C_{12}^2)\bar{u}_{11}^2\}. \quad (23)$$

For brevity, in Eqs. (22a)–(22i) and (23) C_{ijkl} and Q_{ijkl} are expressed in the contracted (Voigt) notation.

The equilibrium values of the polarization in the pseudo-cubic coordinate system follow from the optimization of the modified Landau potential with respect to polarization resulting in the equations of state given by

$$\frac{\partial G_\Sigma}{\partial P_1'} = 2\bar{\alpha}_1 P_1' + 4\bar{\alpha}_{11}P_1'^3 + 2\bar{\alpha}_{12}P_1'P_2'^2 + 2\bar{\alpha}_{13}P_1'P_3'^2 + \beta_1(3P_2'P_1'^2 + P_2'^3) + \beta_2 P_2' + \beta_3 P_3'^2 P_2' - E_1' = 0, \quad (24a)$$

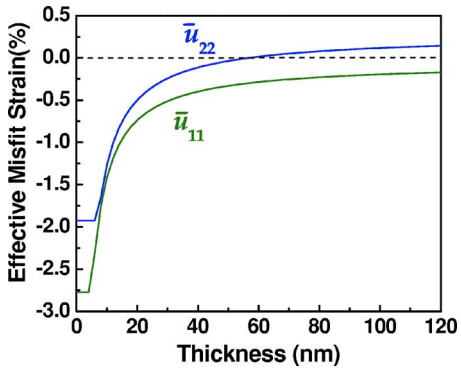

FIG. 2. (Color online) The change of asymmetric misfit strains along $[001]_{BST}$ ($\bar{u}_{11}$) and $[1\bar{1}0]_{BST}$ ($\bar{u}_{22}$) with thickness.

$$\frac{\partial G_\Sigma}{\partial P_2'} = 2\bar{\alpha}_1 P_2' + 4\bar{\alpha}_{11}P_2'^3 + 2\bar{\alpha}_{12}P_2'P_1'^2 + 2\bar{\alpha}_{13}P_2'P_3'^2 + \beta_1(3P_1'P_2'^2 + P_1'^3) + \beta_2 P_1' + \beta_3 P_3'^2 P_1' - E_2' = 0, \quad (24b)$$

$$\frac{\partial G_\Sigma}{\partial P_3'} = 2\bar{\alpha}_3 P_3' + 4\bar{\alpha}_{33}P_3'^3 + 2\bar{\alpha}_{13}P_3'(P_2'^2 + P_1'^2) + 2\beta_3 P_3'P_2'P_1' - E_3' = 0. \quad (24c)$$

Subsequently, to obtain the polarization values in the epitaxial coordinate system (x_1, x_2, x_3), a reverse tensor transformation has to be utilized

$$P_i = a_{ij}^{-1}P_j', \quad (25)$$

where P_j' are the polarization values in the pseudo-cubic coordinate system. After the transformation, the polarization vector is given by

$$P = \begin{bmatrix} P_3' \\ \frac{P_1'}{\sqrt{2}} - \frac{P_2'}{\sqrt{2}} \\ \frac{P_1'}{\sqrt{2}} + \frac{P_2'}{\sqrt{2}} \end{bmatrix}. \quad (26)$$

III. STRAIN STATE AS A FUNCTION OF FILM THICKNESS

To be able to correctly evaluate the polarization behavior, the dielectric response, and the pyroelectric properties, it is crucial to understand the in-plane strain state of the BST 60/40 films. The effective misfit strains of the BST 60/40 film along x_1 ($\bar{u}_{11}$) and x_2 ($\bar{u}_{22}$) as a function of the BST layer thickness are shown in Fig. 2. Below the critical thickness, the strain state corresponds to a pseudomorphic (110) BST layer on (100) NGO. Relaxation starts with misfit dislocation formation along the $[001]_{BST}$ followed by formation of misfit dislocations along $[1\bar{1}0]_{BST}$. Initial compressive misfit strains gradually decrease along both in-plane directions of the film with increasing film thickness [Eqs. (3)–(5)]. However, due to the presence of the thermal strains that arise from the thermal expansion mismatch between the film and the substrate as the film is cooled down from T_G, tensile strains

result above ~57 nm thickness along x_2. This can be explained through the TEC values of BST 60/40 and NGO. Since the TEC of NGO along $[010]_{NGO}$ is smaller than that of BST 60/40 along the corresponding direction, $[1\bar{1}0]_{BST}$ (x_2), the lattice parameter of BST 60/40 along x_2 would decrease more compared to that of NGO along $[010]_{NGO}$ during cooling down above ~57 nm of film thickness leading to tensile strains above this thickness. There is no tensile strain along $[001]_{BST}$ (x_1), since the TEC of NGO along the corresponding direction is bigger than that of BST 60/40 and the residual compressive strain for thicker films is due to the small difference between the TECs along this direction.

IV. POLARIZATION, DIELECTRIC PROPERTIES, AND PYROELECTRIC RESPONSE

The spontaneous polarization in the BST layer can be determined numerically from the simultaneous solution of the equations of state, $\partial G_\Sigma / \partial P_i' = 0$ [Eqs. (24a)–(24c)] for $\bar{u}_{11} - \bar{u}_{22}$ pairs as a function of the film thickness. The dielectric stiffness, elastic, and electrostrictive coefficients used in these calculations were compiled from Ban and Alpay.[12] In our approach, we do not assume *a priori* phase(s) resulting from the loss of symmetry due to the anisotropic internal stress state but seek solutions corresponding to global minimum of the free energy functional from real, positive values of the components of the spontaneous polarization vector as a function of $\bar{u}_{11}$ and $\bar{u}_{22}$.

The dielectric and pyroelectric properties follow from the spontaneous polarization. The small-signal relative dielectric constants can be obtained via

$$\varepsilon_{ii} = \frac{1}{\varepsilon_0} \frac{P_i(E_i = 0) - P_i(E_i)}{E_i}, \tag{27}$$

as $E_i \to 0$ and the dielectric tunabilities along the crystalline axes can be defined as

$$\phi_{ij} = \frac{\varepsilon_{ij}(E_i = 0) - \varepsilon_{ij}(E_i > 0)}{\varepsilon_{ij}(E_i = 0)}. \tag{28}$$

The pyroelectric coefficients due to only the spontaneous polarization are given by

$$p_i = \lim_{\Delta T \to 0} \frac{\Delta P_i}{\Delta T}. \tag{29}$$

Using the effective misfit strains $\bar{u}_{11}$ and $\bar{u}_{22}$ along $[001]_{BST}$ and $[1\bar{1}0]_{BST}$, respectively, the spontaneous polarization in the BST films can be determined via Eqs. (22)–(25). In Fig. 3, we plot the thickness dependence of the spontaneous polarization along $[1\bar{1}0]_{BST}$ (or x_2 and P_2) and $[1\bar{1}0]_{BST}$, (or x_3 and P_3). The in-plane compressive strains favor polarization along the out-of-plane direction $[110]_{BST}$ (P_3) that gradually disappears with increasing thickness due to strain relaxation by the formation of interfacial dislocations and becomes zero at ~85 nm. As for polarization along in-plane directions, P_2 emerges along $[1\bar{1}0]_{BST}$ around ~79 nm after $\bar{u}_{22}$ becomes tensile (~57 nm). The presence of the phase transformation points at ~79 and ~85 nm for P_2 and P_3, respectively, does not immediately follow from the variations in the misfit strains defined in the epitaxial

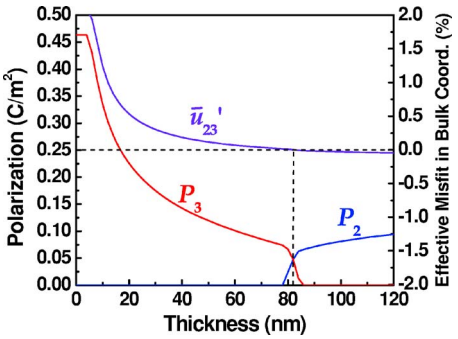

FIG. 3. (Color online) The effect of thickness on the polarizations along $[1\bar{1}0]_{BST}$ (P_2) and $[110]_{BST}$ (P_3) directions. Here, the polarization component along $[001]_{BST}$ (P_1) is equal to zero throughout this thickness range due to compressive strain along this direction. Additionally, corresponding shear strain defined in the pseudo-cubic coordinate system ($\bar{u}_{23}'$) is given to justify the phase transformation at ~80 nm for both polarization components.

coordinates (x_1, x_2, x_3) since there is no significant change in their values around these critical thicknesses. However, if we plot the corresponding shear strain ($\bar{u}_{23}'$) in the pseudo-cubic coordinates (x_1', x_2', x_3') as a function of thickness, as shown in Fig. 3, we observe that this shear strain changes signs at ~83 nm, which justifies the phase transformation for both P_2 and P_3. If we set the value of the "shear strain related" Landau coefficient β_2 zero [Eq. (22h)], the resultant expression is satisfied by the misfit strains defined in the epitaxial coordinates ($\bar{u}_{11}$ and $\bar{u}_{22}$) around these critical thicknesses. For a thickness interval between ~79 and ~85 nm, P_2 and P_3 coexist. There is no spontaneous polarization along $[001]_{BST}$ or x_1 (P_1) in the entire range of thickness since $\bar{u}_{11}$ remains in compression throughout the thickness range that was analyzed.

It can also be seen that the slope of P_3 shows a slight change with the emergence of P_2 around 79 nm and beyond this thickness P_3 decreases more rapidly than its previous trend. The two different in-plane misfits favor the presence of P_2 and P_3 through a range between ~79 and ~85 nm, entirely changing the phase transformation characteristics of the BST 60/40 compared to bulk or films on cubic substrates with the same composition. The existence of polarization components P_3 or P_2 (from Fig. 3, below ~85 nm and above ~79 nm, respectively) and the coexistence of P_2 and P_3 between ~79 and ~85 nm creates structures (or phases) that cannot be realized in films on cubic substrates, which favor two polarization components of equal magnitude along orthogonal axes under tensile strains.[12,26] We note that throughout the thickness range analyzed in this study, the reduction in the point group symmetry caused by the anisotropic in-plane strains will favor a monoclinic ferroelectric phase. Furthermore, the different misfit dislocation densities and thermal strains along $[001]_{BST}$ (x_1) and $[1\bar{1}0]_{BST}$ (x_2) compound this anisotropic polarization behavior. As discussed previously, due to the interplay between the emergence of the tensile strains along $[1\bar{1}0]_{BST}$ caused by the TEC difference and the anisotropic misfit dislocation formation at T_G, the polarization along the out-of-plane direction $[110]_{BST}$ (P_3) starts to diminish and polarization along $[1\bar{1}0]_{BST}$ (P_2) appears. Were the strain along $[1\bar{1}0]_{BST}$ more compressive

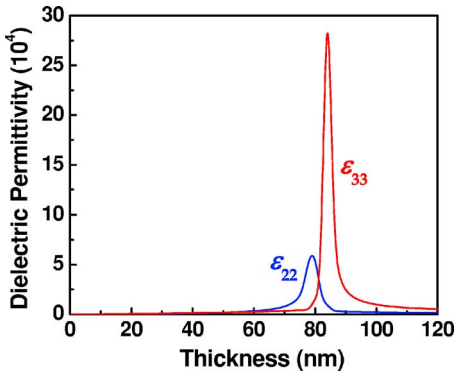

FIG. 4. (Color online) The thickness dependence of dielectric constants along the directions of $[1\bar{1}0]_{BST}$ (ε_{22}) and $[110]_{BST}$ (ε_{33}). Throughout this thickness range, the dielectric constant along $[001]_{BST}$ (ε_{11}) is zero.

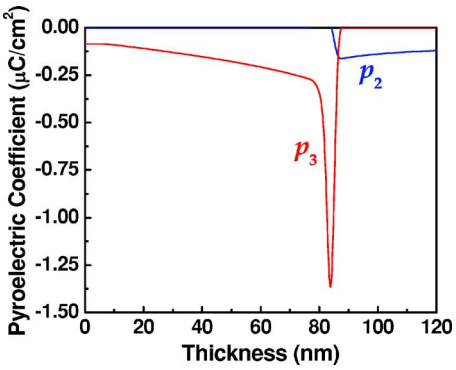

FIG. 6. (Color online) The influence of thickness on the pyroelectric response along $[1\bar{1}0]_{BST}$ (p_2) and $[110]_{BST}$ (p_3) directions. Here, p_1, the pyroelectric response along $[001]_{BST}$ is zero.

throughout the thickness range, P_3 would have persisted at thicknesses above the critical thickness for dislocation formation along this direction.

The dielectric properties of the film can be explained from the polarization behavior as a function of film thickness. Figure 4 plots the small-signal dielectric response as a function of film thickness along in-plane and out-of-plane directions. As expected, due to the strain induced phase transition at two critical thicknesses, ~79 and ~85 nm, we observe a dielectric anomalies along $[1\bar{1}0]_{BST}$ (ε_{22}) and $[110]_{BST}$ (ε_{33}) in the vicinity of these thicknesses, respectively. The dielectric tunabilities along in-plane and out-of-plane directions as a function of BST film thickness for an applied field of 5 kV/mm are shown in Fig. 5. The anomalies in the maximum tunable response along $[1\bar{1}0]_{BST}$ (ϕ_{22}) and $[110]_{BST}$ (ϕ_{33}) are expectedly at ~79 and ~85 nm, respectively, corresponding to the emergence of P_2 at ~79 nm and the disappearance of P_3 at ~85 nm, respectively (Fig. 3). ϕ_{11} is smaller than both ϕ_{22} and ϕ_{33} increases almost linearly with film thickness. This is due to the absence of a spontaneous polarization along $[001]_{BST}$. The tunability is in this case a result of the variation in the induced polarization with the applied electric field. The theoretically calculated values of (ϕ_{33}) of BST 60/40 on NGO are relatively higher even at low film thicknesses compared to the predicted values for BST on isotropic cubic substrates.[14] The tunability findings are in excellent qualitative agreement with the experimental observations of Simon *et al.*, where a similar trend in the out-of-plane tunability was measured as a function of increasing film thickness.[17] However, there is a discrepancy in the film thickness at which the maximum tunability in the out-of-plane direction occurs (≥600 nm). This can be attributed to a number of dynamic factors including the kinetics of formation of misfit dislocations which usually starts at thicknesses significantly larger than the calculated critical thickness[27] and the high frequency of the measurement (in the GHz regime).

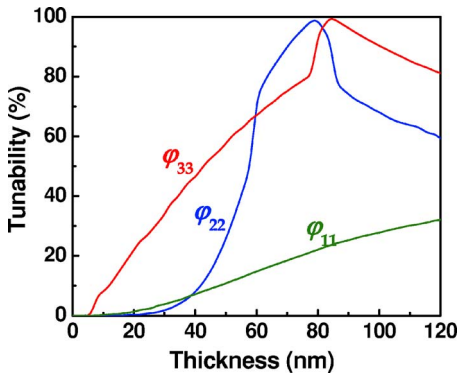

FIG. 5. (Color online) The effect of thickness on tunabilities along three directions ($[001]_{BST}-\phi_{11}$, $[1\bar{1}0]_{BST}-\phi_{22}$, and $[110]_{BST}-\phi_{33}$) of BST 60/40 on NGO.

Pyroelectric response of such films can also be theoretically predicted via Eq. (29). We plot the pyroelectric response for the BST 60/40 film along two major axes of the film as a function of thickness at RT in Fig. 6. Similar to the dielectric response and tunability, abrupt changes in the pyroelectric properties along $[1\bar{1}0]_{BST}$ (p_2) and $[110]_{BST}$ (p_3) can be anticipated at thicknesses where polarization components appear or disappear. As expected, p_2 is more responsive to variations in P_2 and p_3 to variations in P_3. The pyroelectric coefficients predicted at the critical thicknesses are in accordance with the ones predicted for BST films on cubic substrates.[13] Obviously, the benefit of films on anisotropic substrates would be that these high pyroelectric properties can be realized along different in-plane directions.

Furthermore, we can generalize the analysis for any BST film grown on any substrate with the $(110)_{BST}//(100)_{SUB}$, by treating the asymmetric misfit strains as parameters. In Fig. 7, we show three-dimensional plots of the polarization vector as a function of effective misfit strains along the in-plane directions. These plots can be used to predict the effects of anisotropic misfit strain on the phase transformation characteristics, polarization values, and ferroelectric properties. Based on geometric considerations taking into account the polarization and its spontaneous electrostrictive deformation along the corresponding axes, we can conclude that for in-plane effective misfit strain couples where only P_2 or P_3 are present, the crystal structure would be monoclinic. However, in the range where only P_1 is observed, the resulting structure would be tetragonal. In the regions where P_2 and P_3 coexists ($P_2>0, P_3>0$, and $P_2 \neq P_3$), the structure of the film would again be monoclinic due to just in-plane polarization induced deformation. Furthermore, for in-plane effective misfit couples where P_1 and P_2 or P_1 and P_3 can coexist,

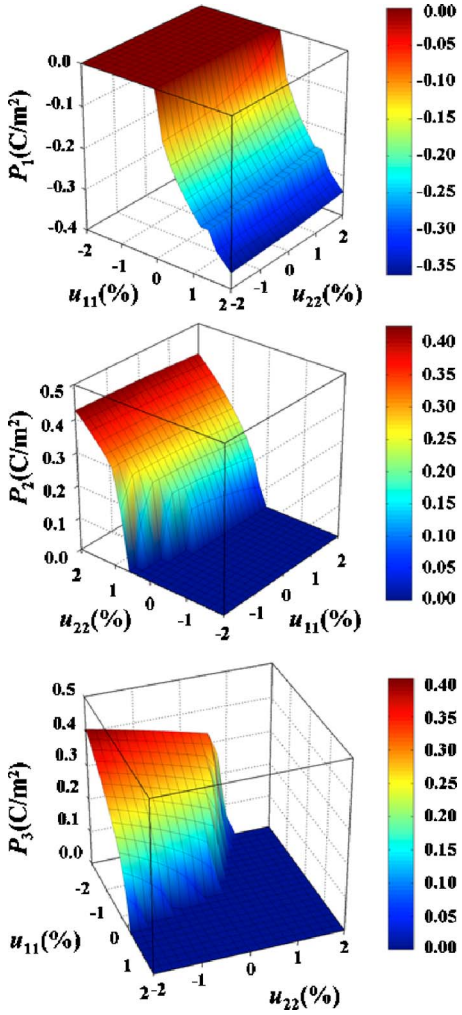

FIG. 7. (Color online) Polarization components along three directions (P_1, P_2, P_3) of the BST 60/40 ferroelectric film as a function of the asymmetric in-plane misfit strains (u_{11}, u_{22}), corresponding to the strain states of different orthorhombic substrates.

the structure would appear to be triclinic as it would be the case in the presence of all three polarization components with $P_1>0$, $P_2>0$, $P_3>0$, and $P_1 \neq P_2 \neq P_3$. None of these phases can be observed in single-crystal prototypical perovskite ferroelectrics such as $BaTiO_3$ (Ref. 28) or BST 60/40 on cubic substrates.[12]

V. CONCLUSIONS

We analyzed theoretically the role of anisotropic in-plane strains on the polarization, dielectric response, tunability, and pyroelectric properties of barium strontium titanate films with (110) epitaxy on (100) orthorhombic substrates. The theoretical model was based on a nonlinear thermodynamic approach that incorporates the formation of misfit dislocations at the film-substrate interface. It was shown that the anisotropic strain resulting from the (110)//(100) epitaxy would result in a point group symmetry reduction in the ferroelectric film that is different than epitaxy on isotropic cubic substrates. This leads to the formation of unique crystal structures (or phases) that cannot be observed in bulk or in films on cubic substrates. Numerical results for (110) BST 60/40 films on (100) NGO show that high dielectric and pyroelectric properties can be achieved via engineering the strain state *along different in-plane directions*. This has significant implications in terms of technological applications as it would provide more flexibility and functionality in terms of device design for elements of DRAMs, frequency-agile microwave electronic components, and thermal imaging systems.

ACKNOWLEDGMENTS

The authors gratefully acknowledge support by the NSF under Grant No. DMR-0132918 and U.S. Army Research Office through Grant No. W911NF-05–1-0528.

[1] S. U. Adikary and H. L. W. Chan, Mater. Chem. Phys. **79**, 157 (2003).
[2] J. A. Bellotti, W. Chang, S. B. Qadri, S. W. Kirchoefer, and J. M. Pond, Appl. Phys. Lett. **88**, 012902 (2006).
[3] C. L. Chen, H. H. Feng, Z. Zhang, A. Brazdeikis, Z. J. Huang, W. K. Chu, C. W. Chu, F. A. Miranda, F. W. V. Keuls, R. R. Romanofsky, and Y. Liou, Appl. Phys. Lett. **75**, 412 (1999).
[4] M. W. Cole, W. D. Nothwang, J. D. Demaree, and S. Hirsch, J. Appl. Phys. **98**, 024507 (2005).
[5] M. W. Cole, W. D. Nothwang, C. Hubbard, E. Ngo, and M. Ervin, J. Appl. Phys. **93**, 9218 (2003).
[6] E. J. Cukauskas, S. W. Kirchoefer, and W. Chang, J. Cryst. Growth **236**, 239 (2002).
[7] J. Im, O. Auciello, and S. K. Streiffer, Thin Solid Films **413**, 243 (2002).
[8] P. C. Joshi and M. W. Cole, Appl. Phys. Lett. **77**, 289 (2000).
[9] E. Ngo, P. C. Joshi, M. W. Cole, and C. W. Hubbard, Appl. Phys. Lett. **79**, 248 (2001).
[10] J. Sok, S. J. Park, E. H. Lee, J. P. Hong, J. S. Kwak, and C. O. Kim, Jpn. J. Appl. Phys., Part 1 **39**, 2752 (2000).
[11] A. Srivastava, D. Kumar, R. K. Singh, H. Venkataraman, and W. R. Eisenstadt, Phys. Rev. B **61**, 7305 (2000).
[12] Z.-G. Ban and S. P. Alpay, J. Appl. Phys. **91**, 9288 (2002).
[13] Z.-G. Ban and S. P. Alpay, Appl. Phys. Lett. **82**, 3499 (2003).
[14] Z.-G. Ban and S. P. Alpay, J. Appl. Phys. **93**, 504 (2003).
[15] W. K. Simon, E. K. Akdogan, A. Safari, and J. A. Bellotti, Appl. Phys. Lett. **87**, 082906 (2005).
[16] W. K. Simon, E. K. Akdogan, and A. Safari, J. Appl. Phys. **97**, 103530 (2005).
[17] W. K. Simon, E. K. Akdogan, A. Safari, and J. Bellotti, Appl. Phys. Lett. **88**, 132902 (2006).
[18] A. G. Zembilgotov, N. A. Pertsev, U. Bottger, and R. Waser, Appl. Phys. Lett. **86**, 052903 (2005).
[19] Y. Lin, X. Chen, S. W. Liu, C. L. Chen, L. Jang-Sik, Y. Li, Q. X. Jia, and A. Bhalla, Appl. Phys. Lett. **84**, 577 (2004).
[20] G. Akcay, I. B. Misirlioglu, and S. P. Alpay, Appl. Phys. Lett. **89**, 042903 (2006).
[21] G. Akcay, I. B. Misirlioglu, and S. P. Alpay, Appl. Phys. Lett. **90**, 036102 (2007).
[22] A. G. Zembilgotov, U. Bottger, and R. Waser, Appl. Phys. Lett. **90**, 036101 (2007).
[23] J. W. Matthews and A. E. Blakeslee, J. Cryst. Growth **27**, 118 (1974).
[24] J. S. Speck, A. C. Daykin, A. Seifert, A. E. Romanov, and W. Pompe, J. Appl. Phys. **78**, 1696 (1995).
[25] S. P. Alpay, V. Nagarajan, A. Bendersky, M. D. Vaudin, S. Aggarwal, R. Ramesh, and A. L. Roytburd, J. Appl. Phys. **85**, 3271 (1999).
[26] N. A. Pertsev, A. G. Zembilgotov, and A. K. Tagantsev, Phys. Rev. Lett. **80**, 1988 (1998).
[27] W. D. Nix, Metall. Trans. A **20A**, 2217 (1989).
[28] F. Jona and G. Shirane, *Ferroelectric Crystals* (Dover, New York, 1962).